Eur. Phys. J. Special Topics **224**, 641–657 (2015)
© EDP Sciences, Springer-Verlag 2015
DOI: 10.1140/epjst/e2015-02397-7

THE EUROPEAN PHYSICAL JOURNAL SPECIAL TOPICS

Regular Article

^{222}Rn and CO_2 at Las Cañadas Caldera (Tenerife, Canary Islands)

M.C. Martin-Luis[1,a], G. Steinitz[2], V. Soler[3], M.L. Quesada[1], and R. Casillas[1]

[1] Universidad de La Laguna, Tenerife, Spain
[2] Geological Survey of Israel, Jerusalem, Israel
[3] Estación Volcanológica de Canarias, IPNA-CSIC, Tenerife, Spain

Received 15 March 2015 / Received in final form 23 April 2015
Published online 10 June 2015

Abstract. Radon, CO_2 and environmental variables are recorded during nearly three years at a shelter hosting a 505 m deep well located close to Teide volcano. Different temporal patterns are observed, annual, semi-annual, semidiurnal and multi-day fluctuations, the latter observed as gradual variation of the semidiurnal signal. CO_2 is anti-correlated with atmospheric pressure at daily and at multiday scale, pointing to a barometric control on the rate of up-flow through the pipe of volcanic CO_2 exsolved from the aquifer. Rn daily maximum lags pressure by 2 hours or more, exhibiting a positive correlation at the multiday scale. Also, an apparent quasi-fortnightly period is detected at Rn, CO_2 and P_{atm} during summer months, with different relations among them (reversal at CO_2 compared to Rn and P_{atm}), pointing to a long period tidal modulation on these gases. Several anomalous large semidiurnal radon peaks were detected, some of them possibly related to seismic events within the volcanic edifice. This work defines radon baseline levels during a period of low geodynamic activity at a site which is in direct contact with a CO_2 saturated aquifer that could be easily perturbed by potential unrests at the central volcanic edifice of the island.

1 Introduction

Tenerife is the largest (2078 km^2) and highest (3718 m) island of the Canarian Archipelago, an intra-plate volcanic chain located about 100 km from the African coast (Fig. 1, inset), and is one of the most complex from the geological point of view. The structure of this island is controlled by a volcano-tectonic rift system forming three axis trending N-E, N-W and N-S, with predominantly basaltic volcanism. The intersection of these three axes is occupied by the large Las Cañadas Caldera (about 16 km the longest axis) which hosts the Teide-Pico Viejo stratovolcano (Fig. 1), both part of the central volcanic complex of Las Cañadas edifice (3.3–0.2 Ma (millions of years before present)), composed by a sequence of basaltic, trachybasaltic,

[a] e-mail: mcmartin@ull.es

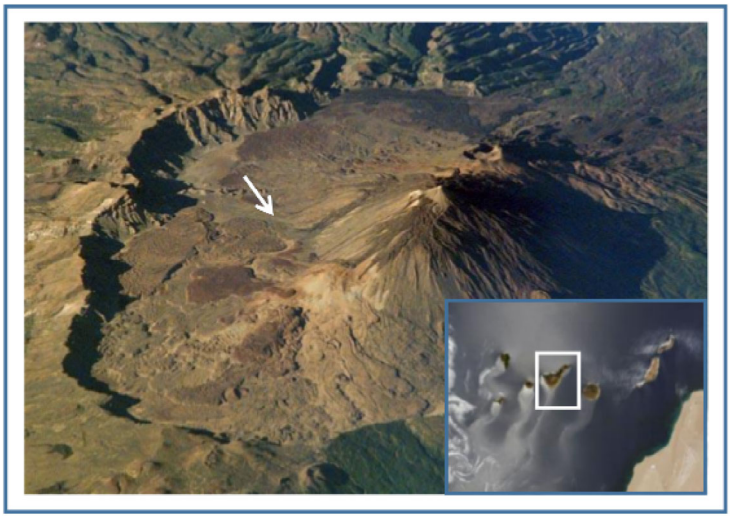

Fig. 1. Location of the monitoring site at Las Cañadas Caldera, Tenerife, Canary Islands (photographic composition from NASA repository).

trachytic and phonolitic products emitted during several constructive and destructive episodes [1,2]. The Teide – Pico Viejo stratovolcano, located inside the caldera depression, is a 3718 m high volcanic complex made of basaltic, trachytic, and phonolitic volcanic products emitted during several eruptive episodes, starting after the Cañadas Caldera formation, (0.2 Ma). The eruptive styles ranged from strombolian to phreatomagmatic activity, cryptodome formation and dome extrusions [2]. The last eruptive event in the terminal crater of Teide took place in 1400 AD [3]. Other historic eruptions occurred along NE and NW axis in 1704, 1705, 1706, 1798 and 1909, mainly consisting of basaltic monogenetic fissural activity [4].

Present day latent volcanic manifestations are the low temperature fumarolic activity at Teide crater ($< 85°C$) and large areas with groundwater thermal and geochemical anomalies in the aquifer of the central zone [5–9]. At this area, CO_2 concentrations up to 10 vol% in air have been measured inside numerous water galleries (water prospection drillings) [5]. During 2004–2005 a seismic crisis occurred at two new seismogenic zones, located NW and SW of the Cañadas Caldera, possibly related to magma intrusion, at least below the NW seismogenic zone [10,11].

Extensive radon mapping at surface (in soil gas) and at the deep subsurface (using the extremely dense network of groundwater galleries existing in the island) revealed large radon anomalies ($> 37000\,Bq/m^3$, background $< 3700\,Bq/m^3$), with a spatial distribution clearly associated with main volcano-tectonic structures of the island. At the central zone, radon anomalies are also associated with areas of high CO_2 emissions and/or areas with thermal anomalies [12]. The temporal variation of radon (^{222}Rn) in the subsurface has also been investigated [7,13–17]. At Tenerife island radon flux patterns significantly differ from one site to another, indicating the influence of the different geological settings and the different degrees of endogenous and environmental variables effects.

In general, radon monitoring performed at different underground sites exhibit (Fig. 2): a) Long term seasonal radon variations, with lower values in winter and higher in summer, b) Non-periodic multi-day (MD) radon signals lasting several days, and c) semi-diurnal radon fluctuations superimposed to the MD signals. The

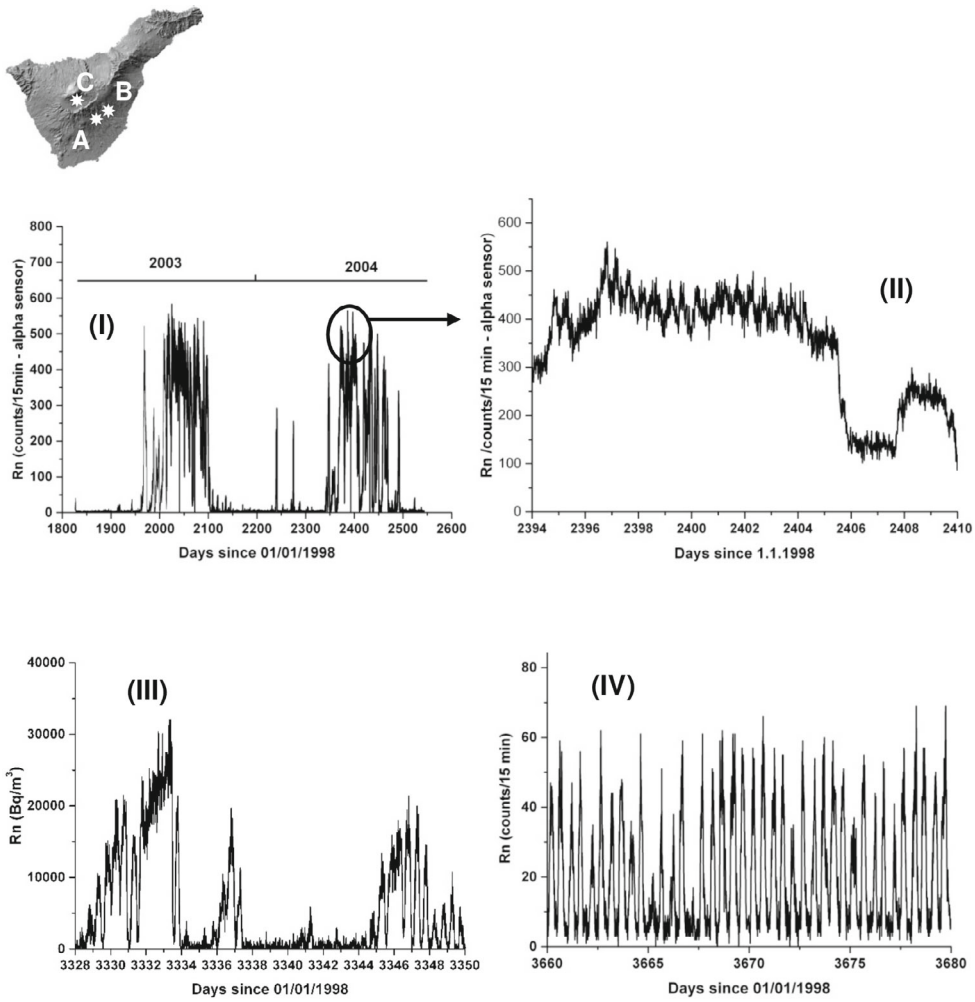

Fig. 2. Radon monitoring at different anomalous zones (up to 7 km apart) (A, B C in map) exhibits different temporal patterns: Long term seasonal variations, with lower values in winter and higher in summer (zone A; Plot I). Non-periodic multi-day (MD) signals (zone B, Plot III; zone A, Plot I), and semi-diurnal radon fluctuations superimposed to the MD signals (zone A, Plot I and II; zone B, Plot III). The amplitude of the semidiurnal variation relative to the MD signal is different and characteristic at each site (Plots II, III, IV).

amplitude of the semidiurnal variation relative to the MD signal is different, systematic and characteristic for each site.

One of these sites (Montaña Majua, Fig. 2C) exhibits mainly semidiurnal fluctuations, and MD signals defined by the gradual variation of the daily maxima. Non-periodic MD radon fluctuations have been frequently associated to geological activity (seismic/volcanic/rock mass deformation) [18–26]. Diurnal and semidiurnal radon variations have been studied in relation to many other periodic phenomena (barometric pressure, atmospheric temperature, Earth tide deformation, solar irradiance) as possible drivers for radon variation [20,27,28,30–33], but no clear consensus exists.

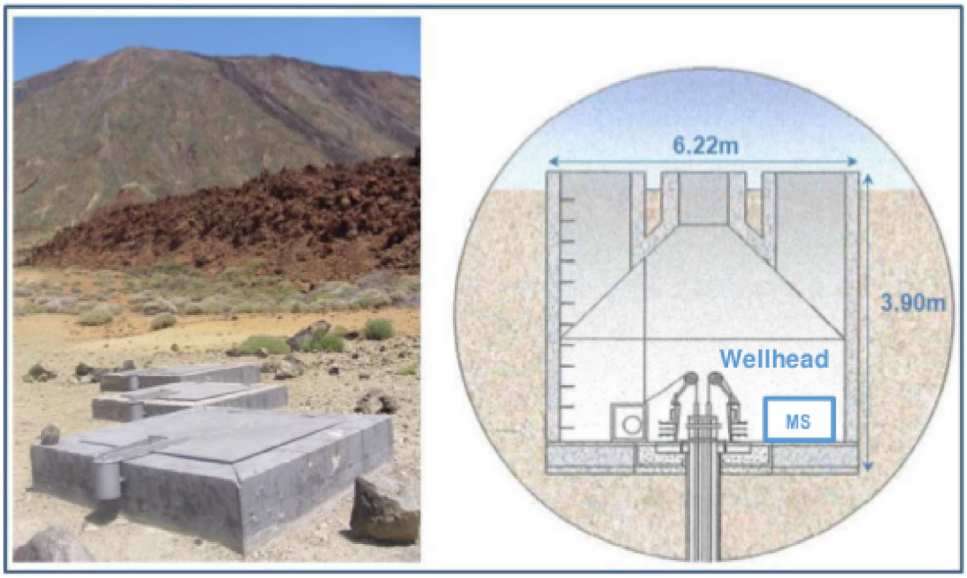

Fig. 3. Shelter entrance (left) and vertical layout of the underground structure (right, modified from [34]). The monitoring station (MS) is located inside the shelter, next to the wellhead. Radon, CO_2, barometric pressure and internal air temperature are measured at this point. External air temperature is measured outside the shelter, about 50 m apart.

In this work we combine radon measurements with the simultaneous monitoring of another gas – CO_2, and environmental variables (air temperature and barometric pressure) in order to better understand the daily and multiday radon signals in the context of the active volcanism of Tenerife. Nearly three years long time series are analysed and compared to the recorded seismic activity in the island.

2 Experimental site and analytical procedure

Montaña Majua site is a 505 m deep well used for hydrogeological research by the Water Council of Tenerife (Consejo Insular de Aguas de Tenerife). This facility is located at 2264 m above sea level in the central area of Las Cañadas Caldera, at about 600 m from the South-eastern base of Teide volcano (Fig. 1). The lithology along the borehole corresponds to an upper layer of phonolitic and pumiceous rocks followed by basaltic lavas and some intermediate trachybasaltic flows that belong to the Teide-Pico Viejo sequence [35]. A more detailed description of the lithological column of this well is given in [7]. The wellhead is hosted into a shelter that is partially isolated from the external air by three metallic doors (Fig 3). The water level inside the well (unconfined aquifer) is around 446 m depth. Inside the well, CO_2 concentrations up to 40 % in volume have been measured between the water table and a zone of thermal inversion located around 300 m depth [7]. The CO_2 is of volcanic origin and is released from the CO_2 saturated aquifer.

Radon, CO_2 and environmental variables (air temperature and barometric pressure) are recorded during nearly three years inside the shelter, next to the wellhead (Fig. 3), by using a multi-parametric station consisting of: a) a radon measurement system based on a Geiger-Müller counter (RM-70 detector, Aware, USA) sensitive to alpha, beta and gamma radiation, as well as X-ray radiation above 10 keV, b) a

non-dispersive infrared (NDIR) sensor (SenseAirTM, Sweden) with a measurement range from 0 to 4% vol for CO_2 measurements, c) a temperature sensor (PT100) and d) a PTB100 analog barometer (VAISALA, Finland). All are connected to a datalogger using a time resolution of one hour. Overlapping comparative measurements of radon in the shelter are done with a radon probe (Barasol, Algade Inc., France), (silicon detector for α particles, sensitivity of 1 cph (= about 50 Bq/ m^3), with a sampling interval of 15 minutes. Outside the shelter and about 50 m apart, external air temperature and relative humidity are recorded using a HOBO Temp/RH datalogger (ONSET Corp., USA).

Decimal time (UT; day 0 = 1.1.1998) is used for the obtained time series, that span from February 14, 2013 to September 30, 2014 with the Barasol probe and from February 10, 2012 to September 30, 2014 for the rest of instruments. Raw data from the Barasol probe (radon – alpha) and external temperature sensor were decimated from the original 15 min. time resolution to one hour. Data gaps of three hours or less were filled by linear interpolation. A six day gap existing at the Barasol record from July 2 to 7, 2014 was retained.

The obtained times series are analyzed in the time and frequency domains, at different time scales and intervals: Long term (multiyear) trend is analyzed by simple linear regression of the time series. The residuals of the linear regressions are further used for analysis of the de-trended time series. Seasonal/annual variability is obtained by FFT filtering using a 45 day window. Several smoothing methods using different window lengths were performed to select this optimal procedure. Shorter periodic components are extracted by FFT analysis of the de-trended time series. Phase variability of the diurnal components is studied by frequency histograms of the daily maxima. Observed anomalous intervals are later compared to the seismicity recorded within a radius of 40 km from the monitoring site. Seismicity recorded during the observational period is obtained from the National Geographical Institute catalog (`http://www.ign.es/ign/layoutIn/volcaFormularioCatalogo.do`).

3 Results

The long-term temporal variation of ^{222}Rn, CO_2, barometric pressure, internal and external air temperature is shown in Fig. 4. A statistical summary of the data is given in Table 1. Radon concentration in Bq/m^3 is given by the calibrated Barasol probe and can be qualitatively compared to the count level obtained with the Geiger-Müller.

The mean radon concentration inside the shelter during the monitored period is of 7944 Bq/m^3, well above the mean continental concentration in open air (10–30 Bq/m^3), with maximum values higher than 22,000 Bq/m^3. CO_2 concentration varies from 0.2 to near 4% in volume.

A detail with two examples of 10 days and one month time windows can be observed in Fig. 5. Semi-diurnal signals are evident in Rn, CO_2 and P_{atm}. Rn daily signals lag by 2h (up to 5 h) the daily CO_2 fluctuations (Fig. 5a, b). Occasionally, Rn anomalies occur, defined as large semidiurnal radon peaks, usually not accompanied by CO_2 peaks (Fig. 5b). These radon anomalies are studied in more detail in Sect. 3.4. At a larger time scale, multiday patterns (MD), defined by the gradual variation of the daily signal, can be observed in Rn, CO_2 and P_{atm}. (Fig. 5c and d). Variable relations are observed between MD-Rn and MD-CO_2 and also between each gas and MD-P_{atm}. MD-CO_2 are mostly anti-correlated to MD-P_{atm} (as expected), however during some intervals MD-Rn are positively related to P_{atm} (Fig. 5c). In other occasions, though MD-Rn and MD-CO_2 events coincide in the same time interval, their upper envelopes exhibit inverse patterns (Fig. 5d).

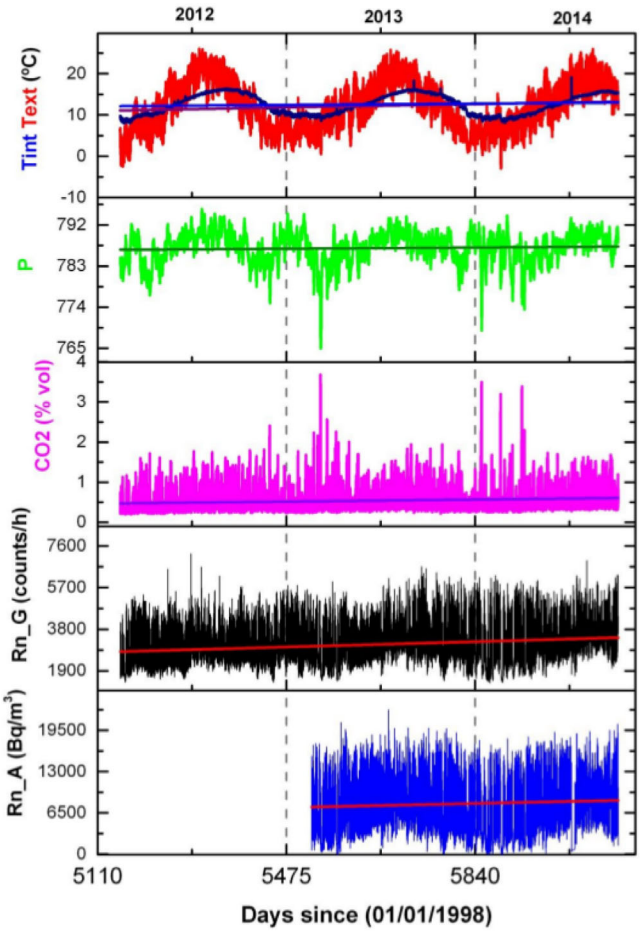

Fig. 4. Temporal variation (from top to bottom) of external (T_{ext}) and internal temperature (T_{int}), barometric pressure, CO_2, radon counts at the GM sensor and ^{222}Rn at the Barasol probe, from February 2012 to September 2014. Long term (multiyear) trends defined by linear regression fits are also showed.

3.1 Long-term (multi-year) variation

All variables exhibit a positive increasing trend (Fig. 4). The increase is almost negligible in CO_2 (slope 1.37×10^{-4}), P_{atm} (slope 7.18×10^{-4}) and T_{int} (slope 8.62×10^{-4}) and it is small in T_{ext} (slope 0.002). A faster increasing trend is recorded at Rn (slope Rn GM 0.67), and especially at Rn-alpha (slope 1.76). Multiyear increasing trends in radon levels have been interpreted as due to the influence of the long-lived radon decay product Pb-210 (half-live of 22.3 yr) [28].

3.2 Seasonal/annual variability

Seasonal/annual variability is obtained by FFT filtering using a 45 day window (Fig. 6). Seasonality is evident at all parameters, being strongest at T_{ext} and T_{int} and less clear at Rn gamma. Also, during 2013 (the only complete year) a semi-annual pattern can be observed in CO_2, Rn gamma and barometric pressure.

Table 1. Descriptive statistics of the time series.

Parameter	Mean	Min.	Max.	% St.Dev.
Rn-GM (counts/h)	3095	1350	7251	31.3
CO_2 (% vol.)	0.5	0.2	3.7	63.0
P (mbar)	786.9	764.9	795.5	0.4
T_{int} (°C)	12.6	8.0	19.1	19.0
T_{ext} (°C)	12.2	−3.0	26.1	47.5
Rn-A (Bq/m^3)	7944	0	22770	60.0

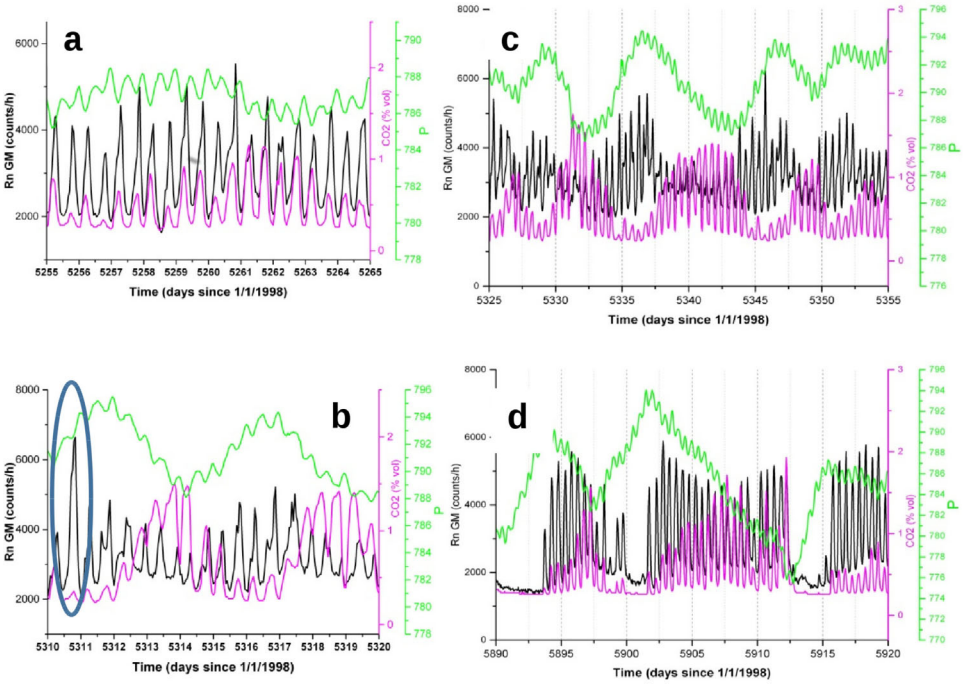

Fig. 5. Two examples of 10 days (a, b) and one month time windows during summer (c) and winter (d). Semi-diurnal signals are evident for Rn, CO_2 and P_{atm} (a, b). Rn daily signals lag by 2 h (up to 5 h) the daily CO_2 fluctuations (a, b). Occasionally, Rn anomalies occur, defined as large semidiurnal radon peaks usually not accompanied by CO_2 peaks (ellipse in b). Multiday patterns (MD) defined by the gradual variation of the daily signal, are observed at Rn, CO_2 and P_{atm}. (c and d).

At all parameters annual maxima occur during summer and the annual minima during winter, however there are different time lags among them. Using the time of the external air temperature summer maxima as reference, the only stable time lag occurs between T_{int} and T_{ext} (T_{int} summer maxima is 35 days lagged) but this lag varies for Rn and CO_2 (Table 2). Therefore T_{ext} doesn't seem to have a relevant influence on radon or CO_2 levels at this site at a yearly scale.

3.3 Daily fluctuations

Figure 7 presents the power spectra of the signals filtered at the daily frequency band. Both ^{222}Rn and CO_2 have spectral patterns very similar to that of P_{atm},

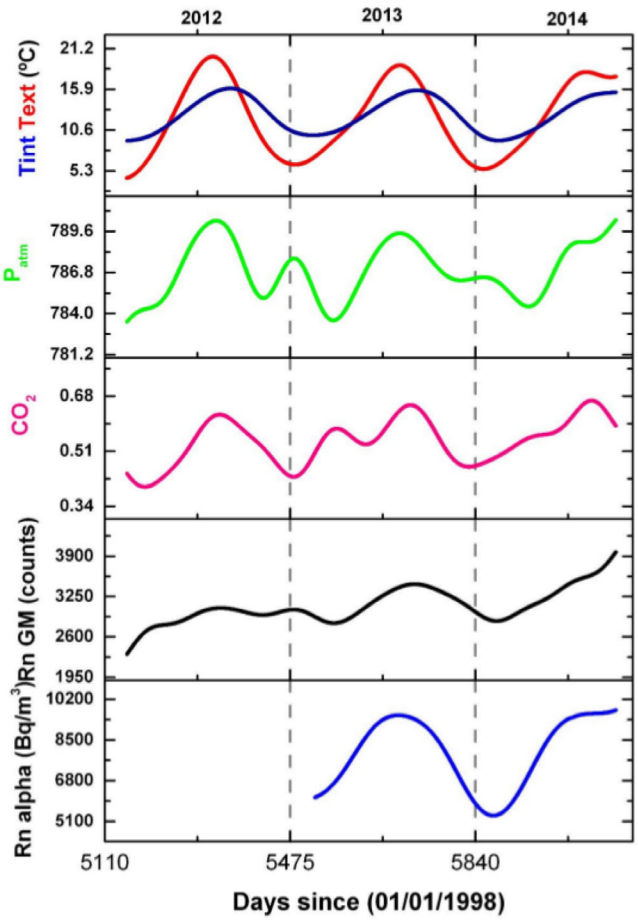

Fig. 6. Seasonal variability (from top to bottom) of external temperature (T_{ext}) and internal temperature (T_{int}), barometric pressure (P), CO_2, Rn-gamma and Rn-alpha.

Table 2. Time lag between the seasonal variation of external temperature (T_{ext}) and the other variables.

	2012 lag (days)	2013 lag (days)
T_{int}	35	34
Rn-alpha		+3
Rn GM	16	29
CO_2	14	21
P_{atm}	7	0

with a strong S2 constituent (12 h), minor S1 (24 h) and S3 (8 h). S4 (6 h) is also present in the spectra for Rn gamma, Rn alpha and barometric pressure. This spectral content is very different from that of the external atmospheric temperature which has a dominant S1 periodicity. Therefore, as for the seasonal variation, at a daily scale Text doesn't seem to have a relevant influence on radon or CO_2 levels.

Phase variability is studied by analysing the frequency histograms of the daily maxima at each variable and in two periods, winter and summer. In this analysis, winter and summer periods have been defined taking into account the relation between the external and internal air temperature, considering the two most extreme

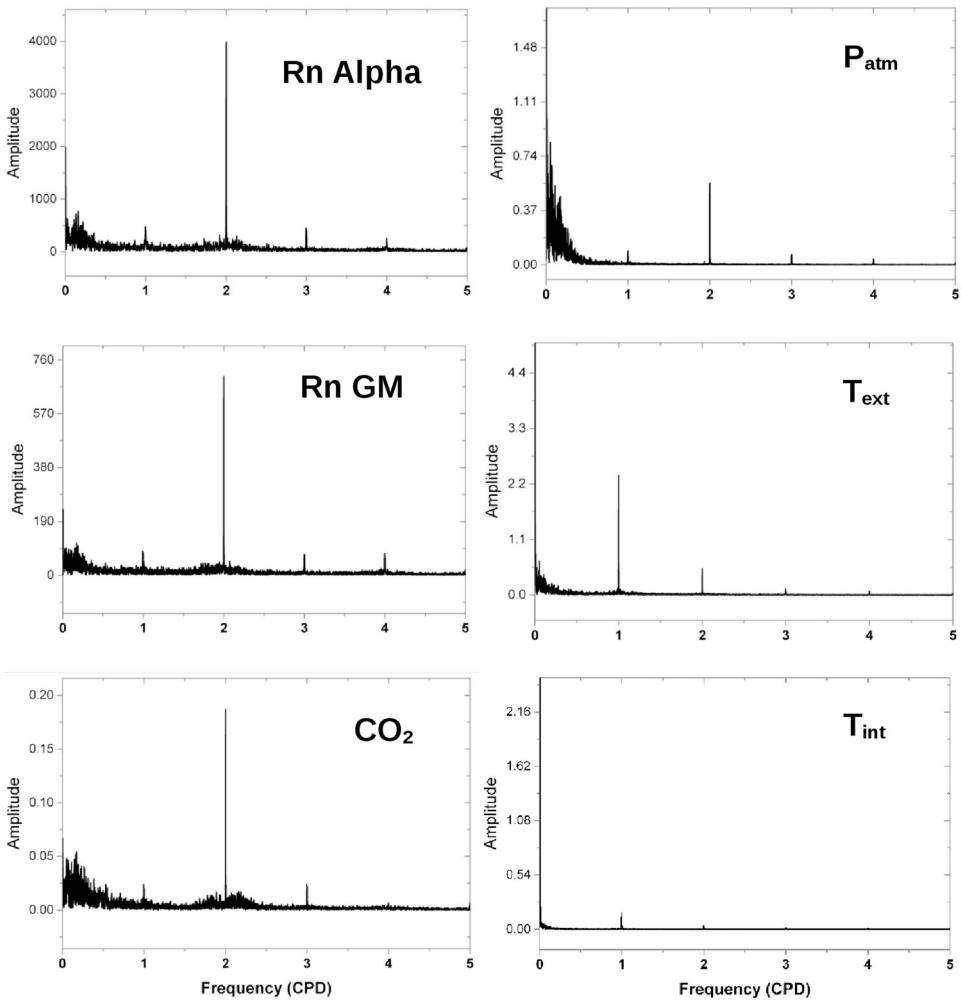

Fig. 7. Fourier spectra of the de-trended time series.

intervals as described in Fig. 8. Winter interval spans from October 24, 2013 to January 17, 2014, a period where the air temperature inside the shelter is mostly above the external one. Summer interval spans from June 28, 2014 to September 19, 2014, when the temperature outside is most of the time above the internal one.

The phases of daily variations of external temperature (T_{ext}) and barometric pressure (P_{atm}) are stable through the year, with peak times around 16:00 h for atmospheric temperature and at 12:00 and 23:00–24:00 h for barometric pressure. The same is for CO_2, with stable semidiurnal peak times around 7:00–8:00 and 17:00–19:00 h through the year. In winter, CO_2 and radon are in phase most of the time and both are in anti-phase with atmospheric pressure (as expected). However, during summer, the radon phase shifts up to 4 hours, resulting in semidiurnal peak times around 9:00 and 22:00 h, being almost in phase with barometric pressure (Fig. 9). Thus, at a daily scale, the barometric tide seems to be the main driver for the semidiurnal variation at CO_2, but the varying time shift along the year of the semidiurnal radon signal compared to the stable phase of CO_2 and P_{atm} makes the relation of radon with barometric pressure deceptive.

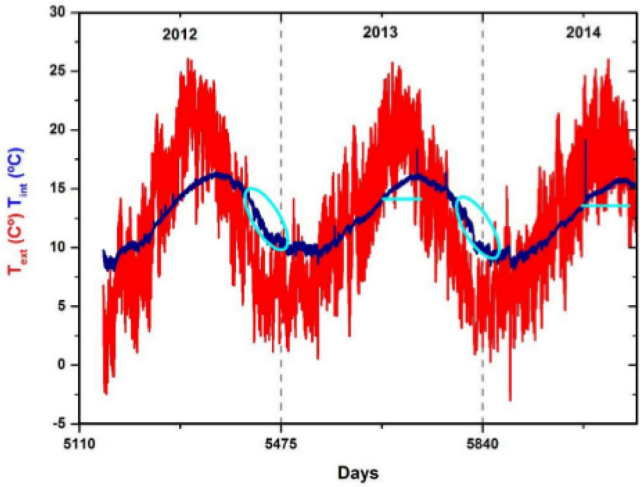

Fig. 8. For the analysis of the daily and multiday variations, winter and summer periods have been defined taking into account the relation between the external and internal air temperature, considering the two most extreme intervals. The winter interval spans from October to January, a period where the air temperature inside the shelter is mostly above the external one (ellipse). The summer interval spans from ends of June to September, when the temperature outside is most of the time above the internal one (horizontal line).

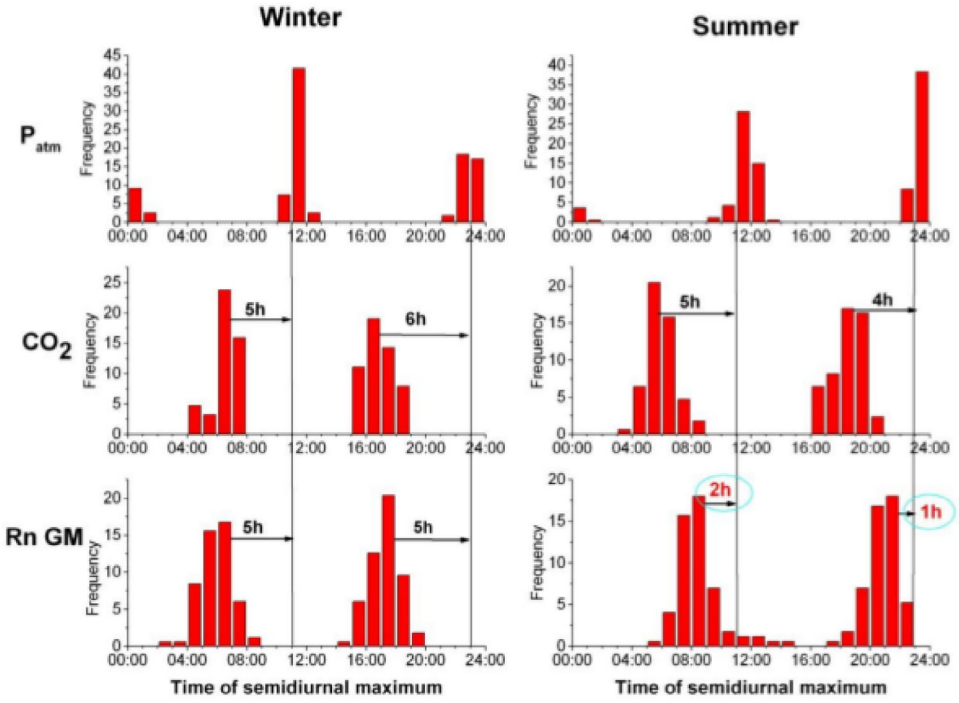

Fig. 9. Frequency histograms of the daily maxima of ^{222}Rn, CO_2 and P_{atm} in two periods, winter (from October 24, 2013 to January 17, 2014) and summer (from June 28 to September 19, 2014). In winter, CO_2 and radon are in phase most of the time and both are in anti-phase with atmospheric pressure. During summer, radon phase shifts up to 4 hours, being almost in phase with barometric pressure.

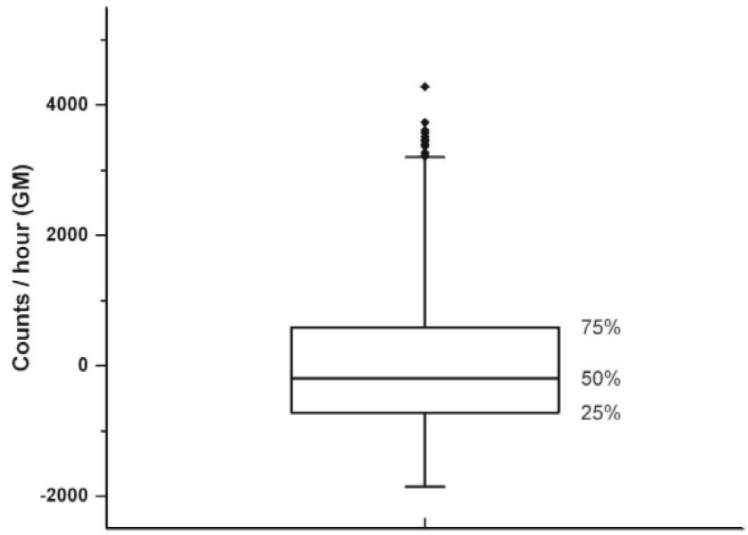

Fig. 10. Box plot of the de-trended and de-seasoned radon time series. Radon anomalies (outliers set as two times the inter-quartile range above the third quartile), are defined as radon levels higher than 3198 counts.

3.4 Radon anomalies

Rn anomalies, defined from the de-trended and de-seasoned radon time series as semidiurnal peaks reaching a count number larger than two times the inter-quartile range above the third quartile (see outliers in the box plot of Fig. 10 and an example of anomaly in Fig. 5b), are compared to the seismic activity recorded during the observational period, within a radius of 40 km from the monitoring site. 78 seismic events were recorded from 30/01/2012 to 01/10/2014, with magnitudes between 0.8 and 3.8. Eight radon anomalies were determined, all of them corresponding to the second semidiurnal peak. Three of these anomalies occurred between 1.5 and 4 days after a seismic event, one occurred one day before, one was in the same day and three anomalies occurred without any seismicity being recorded in the 5 days before or after. The magnitude of these possibly related seismic events ranged from 1.3 to 2.5

Some of these radon anomalies seem to be related to the occurrence of seismic events within the volcanic edifice. However, similar seismic events have not resulted in radon anomalies, lowering the significance of the observations. Influences of meteorological variables such as rainfall or snow cover have been ruled out as Las Cañadas Caldera is an arid zone, with less than 300 mm of rain per year, and most of the radon anomalies have occurred during the driest months (May to September). On the other hand, CO_2 variations do not show any relation to the seismic activity during the observed period.

3.5 Non-periodic multiday (MD) variation

Non-periodic multiday signals (MD), defined by the gradual variation of the daily fluctuations, can be observed in Rn, CO_2 and P_{atm}. (Fig. 5c and d). Variable time

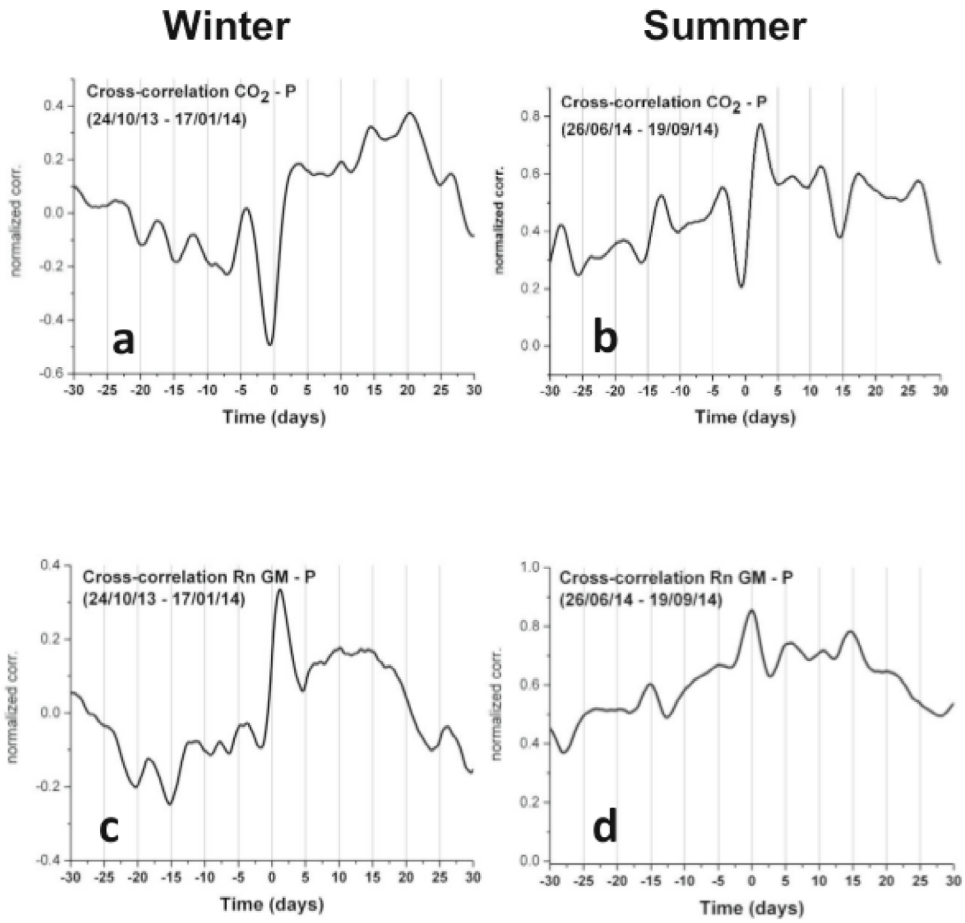

Fig. 11. Cross-correlation analysis (using Origin software, OriginLab Corp.) between the upper envelopes of the de-trended time series at two intervals, winter and summer. CO_2 and P_{atm} MD variations are anti-correlated with a small lag of 0.5 day (CO_2 lagged), (a and b). Rn and P_{atm} MD variations are positively correlated, with a time lag varying from zero in summer to +1 day in winter (P_{atm} lagged), (c and d).

shifts are observed between MD-Rn and MD-CO_2 and also between MD-Rn and MD-P_{atm}. Time lags among MD Rn, CO_2 and P_{atm} were calculated by cross-correlation analysis between the upper envelopes of the de-trended time series (Fig. 11). Due to the observed Rn diurnal phase shifts along the year and the variable MD-Rn relation to MD-P_{atm} (and CO_2), the cross-correlation analysis was also performed at two different intervals, in winter and in summer, as defined in Sect. 3.3.

CO_2 and P_{atm} MD variations are anti-correlated with a small lag of 0.5 day (CO_2 lagged), which is constant through the year (Fig. 11a) and b)). Conversely to what could be expected if radon is driven by volcanic CO_2, Rn and P_{atm} MD variations are positively correlated, with a time lag varying from zero in summer to +1 day in winter (P_{atm} lagged) (Fig. 11c) and d)). Also, from the cross-correlation functions in Fig. 11, an apparent quasi-fortnightly period is detected at Rn, CO_2 (Fig. 12a) and P_{atm} (Fig. 12b) during summer months, with different relations among them (reverse CO_2 variations compared to Rn and P_{atm}). This periodicity is absent during winter.

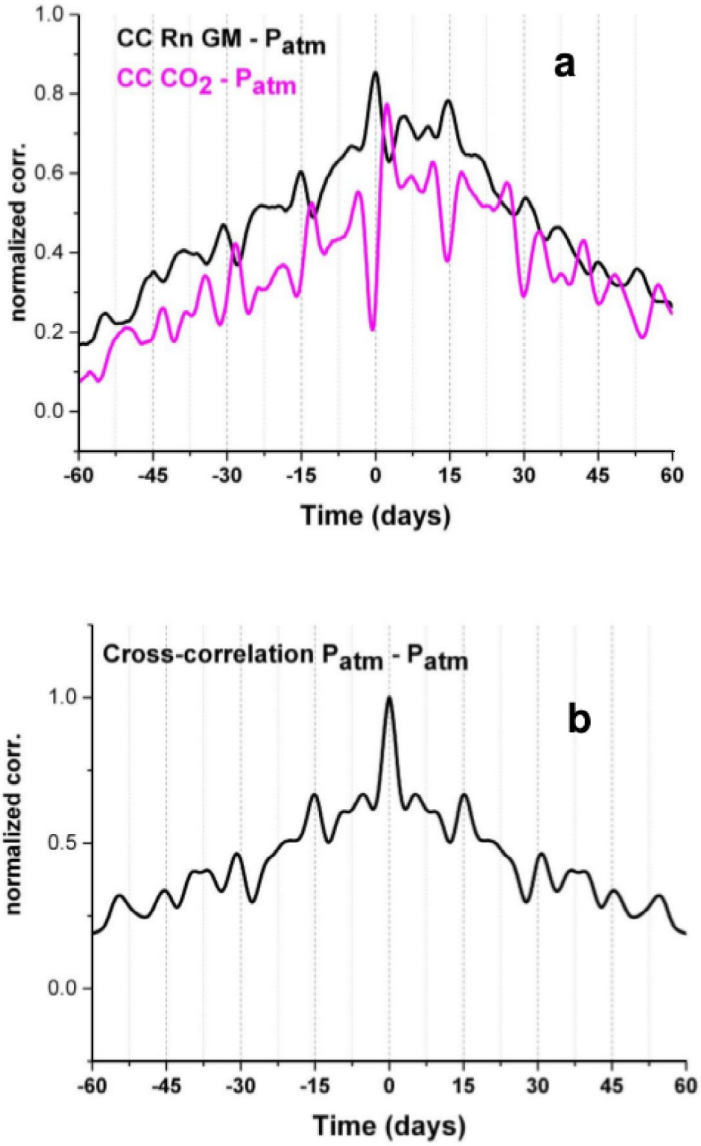

Fig. 12. Cross-correlation diagrams for Rn vs. P_{atm} and CO_2 vs. P_{atm} (a), and for P with itself (b) during summer months. An apparent quasi – fortnightly period is detected with different relations among them (reversal at CO_2 compared to Rn and P_{atm}).

This could be an indication on a long period tidal modulation on these gaseous components.

Also in this case, it could be assumed that the temperature gradient between the external ambient temperature and the internal one in the shelter, has a complex effect which is reflected in a gradual variation of multiday radon patterns during the year, which could be related to a variable rate of natural ventilation of the shelter. During winter, when external air temperature is mostly below the internal one, cooler and denser radon free air can enter into the shelter diluting radon concentration

and influencing radon variation patterns, making them more similar to those of CO_2 (Fig. 5d). During summer, external air temperature is mostly above the internal one, avoiding or minimising the thermal ventilation effect, resulting in relatively isolated conditions and thus in a better observational situation to analyse pure degasification/emanation phenomena (Fig. 5c). This could be also an explanation of the fact that radon anomalies are more frequently detected during summer and to the lack of fort-nightly periodicity during winter months.

4 Discussion and conclusions

Radon, CO_2 and environmental variables (air temperature and barometric pressure) are recorded during nearly three years at Montaña Majua site, a key location for volcanic surveillance due to its location, close to base of Teide volcano, and to its long term accessibility as a governmental facility.

At this site, several temporal patterns are observed in both gases: annual and semi-annual modulation, prominent semidiurnal fluctuations and multi-day variations formed by the gradual variation of the semidiurnal signal during intervals of several days.

Comparison to environmental variables highlights differences between both gases at different time scales. At a daily scale, the barometric tide seems to be the main driver for the semidiurnal variation of CO_2, and possibly also of radon. However, radon daily maximum lags pressure by 2 hours or more, and exhibits a positive correlation with pressure at the multiday scale. The varying time shift along the year of the semidiurnal radon signal compared to the stable CO_2 and P_{atm} makes the relation of radon with barometric pressure deceptive.

At larger time scales (weekly-monthly), there is also a reversed relation between CO_2 and barometric pressure, with a small lag of about half a day, which is consistent along the year. For radon the correlation with pressure is positive, with a varying time shift between 0 in summer and +1 day in winter. As far as known, there is no mechanism that can explain an increased radon emanation or flux under positive barometric pressure gradients.

Based on the different temporal patterns observed for each gas, different sources for radon (mainly the surrounding shelter walls) and CO_2 (barometric pressure driven groundwater degassing and advective flow through the pipe of the well) are suggested. This is also supported by the fact that the larger CO_2 peaks (>2% in vol) are systematically accompanied by strong barometric pressure drops. In these cases it is possible that during stormy (very low pressure) weather, the so called "mountain breathing" phenomena described by Woodcock driven by a combination of Bernoulli effect of strong winds and barometric pressure drop [36], could be acting at this high volcano (measurements are done at 2150 m above sea level), resulting in a more effective transport of CO_2 through the borehole to the surface. But this is not the case for radon, as these large CO_2 peaks are not accompanied by proportional radon increases and conversely, large radon peaks described in this work as anomalies, are not accompanied by similar CO_2 increases. Thus we conclude that at Montaña Majua well radon and CO_2 have different dynamics and sources.

Moreover, an apparent quasi-fortnightly period is detected in Rn, CO_2 and P_{atm} during summer months, with different relations among them (reverse CO_2 variations compared to Rn and P_{atm}). This could be an indication on a long period tidal influence on these gaseous components. If this is the case, gravity tide driving Earth tidal deformation would be causing tidal changes in radon emission with the same quasi-15 day period and phase. At the same time, the quasi-fortnightly barometric tide [37,38] would be driving CO_2 flux variations through the pipe well with the same

periodicity but with opposite phase. Longer time series would be needed to support this hypothesis.

Radon anomalies, extracted from the de-trended and de-seasoned radon time series, were compared to the seismic activity during the observational period within a radius of 40 km. Eight anomalies were detected, all of them corresponding to the second semidiurnal peak. Influences of meteorological variables such as rainfall or snow cover have been ruled out as Las Cañadas Caldera is an arid zone, with less than 300 mm of rain per year, and most of the radon anomalies have occurred during the driest months (May to September). Some of these radon anomalies seem to be related to the occurrence of seismic events within the volcanic edifice. However, similar seismic events have not resulted in radon anomalies, and also there are radon anomalies without any seismic event counterpart, resulting in an ambiguous interpretation. Further analysis taking into account the different seismogenic zones within the island would be needed to better define whether a relation exists. In turn, CO_2 variations do not show any relation to the seismic activity during the observed period.

On the other hand, the temperature gradient between the external temperature and the internal one at the shelter seems to have a complex effect which is reflected in a gradual variation of multiday radon patterns during the year. A possible explanation for this phenomenon could be related to a variable rate of natural ventilation of the shelter, higher in winter and lower in summer, resulting in more isolated conditions during the summertime and thus in a better observational situation to analyse pure degasification/emanation phenomena. This could be also an explanation for the observation that radon anomalies are more frequently detected during summer intervals and to the lack of fort-nightly periodicity during winter months. An improvement of the experimental configuration including, for instance, flow rate and wind speed measurements would provide complementary information for a better understanding of the different gas dynamics and is recommended for future research.

Moreover, the described data reflect complex phenomena and part of them are not well understood, especially concerning radon, not only due to the complexity of the environmental interactions but possibly also to complexities related to the nature of its radioactive decay [32,33,39].

Radon monitoring at the Montaña Majua site started several years after the seismic crisis occurred in Tenerife in 2004–2005. The seismicity in the island has decreased since then and, in spite of few apparently related radon anomalies, no clear relationship is observed between radon and present-day seismic activity. On the other hand, the recent volcanic eruption at El Hierro island [24,25] evidenced the need to know the baseline levels during quiescence periods. In this sense, this work contributes to establish radon levels during a period of low geodynamic activity at a key site which is in direct contact with a CO_2 saturated aquifer that could be easily perturbed by potential unrests at the central volcanic edifice of the island.

This study has been supported by the Spanish Projects CGL2010-17148, CGL2009-07775/BTE, PI2008-250, CGL2011-25494 and CGL12-33430. We are grateful to the Water Council of Tenerife (Consejo Insular de Aguas, Cabildo de Tenerife) for providing access to their facility at Montaña Majua borehole. We are also grateful to two anonymous referees for their careful reading and valuable suggestions.

References

1. E. Ancochea, J.M. Fuster, E. Ibarrola, A. Cendrero, J. Coello, F. Hernán, J.M. Cantagrel, C. Jamond, J. Volcanol. Geotherm. Res. **44**, 231 (1990)
2. G.J. Ablay, J. Martí, J. Volcanol. Geotherm. Res. **103**, 175 (2000)

3. X. Quidelleur, P.Y. Gillot, V. Soler, J.C. Lefèvre, Geophys. Res. Lett. **28**, 3067 (2001)
4. J.C. Carracedo, E. Rodríguez, H. Guillou, M. Paterne, S. Scaillet, F. Pérez, R. Paris, U. Fra-Paleo, A. Hansen, GSA Bulletin **119**, 1027 (2007)
5. A. Valentin, J.F. Albert-Beltran, J.L. Diez, J. Volcanol. Geotherm. Res. **44**, 251 (1990)
6. I. Farrujia, P. Delgado, J. Fernández, in *Proceedings Congreso Análisis y Evolución de la Contaminación de las Aguas Subterráneas* (AIH, 1994) p. 397
7. V. Soler, J.A. Castro Almazá, R.T. Viñas, A. Eff-Darwich, S. Sánchez Moral, C. Hillaire Marcel, I. Farrujia, J. Coello, J. De La Nuez, M.C. Martin, M.L. Quesada, E. Santana, Pure Appl. Geophys. **161**, 1519 (2004)
8. A. Eff-Darwich, J. Coello, R. Viñas, V. Soler, M.C. Martin-Luis, I. Farrujia, M.L. Quesada, J. de la Nuez, Pure Appl. Geophys. **165**, 1355 (2008)
9. R. Marrero, D. López, P. Hernández, N. Pérez, in *Terrestrial Fluids, Earthquakes and Volcanoes: The Hiroshi Wakita Volume III*. Pageoph Topical Volumes (2008), p. 147
10. I. Domínguez – Cerdeña, C. del Fresno, L. Rivera, J. Volcanol. Geotherm. Res. **206**, 15 (2011)
11. I. Prutkin, P. Vajda, J. Gottsmann, J. Volcanol. Geotherm Res. **282**, 9 (2014)
12. M.C. Martin-Luis, Ph.D. thesis, Universidad de La Laguna, 1999
13. C. Martin-Luis, M.L. Quesada, A. Eff-Darwich, J. De la Nuez, J. Coello, A. Ahijado, R. Casillas, V. Soler, Environ. Geol. **43**, 72 (2002)
14. A. Eff-Darwich, C. Martin-Luis, M.L. Quesada, J. de la Nuez, J. Coello, Geophys. Res. Lett. **29**, 261 (2002)
15. G. Steinitz, C. Martin, N. Gazit-Yaari, M.L. Quesada, J. de la Nuez, R. Casillas, U. Malik, Z.B. Begin, Appl. Radiat. Isotopes Appl. Radiat. Isotopes **64**, 520 (2006)
16. R. Viñas, A. Eff-Darwich, V. Soler, M.C. Martin-Luis, M.L. Quesada, J. de la Nuez, Radiat. Meas. **42**, 101 (2007)
17. A. Eff-Darwich, R. Viñas, V. Soler, J. de la Nuez, M.L. Quesada, Radiat. Meas. **43**, 1429 (2008)
18. G. Steinitz, Z. Begin, N. Gazit-Yaari, Geology **31**, 505 (2003)
19. Y. Yasuoka, Y. Kawada, Y. Omori, H. Nagahama, T. Ishikawa, S. Tokonami, M. Hosoda, T. Hashimoto, M. Shinogi, Appl. Geochem. **27**, 825 (2012)
20. P. Richon, J.C. Sabroux, M. Halbwachs, J. Vandemeulebrouck, N. Poussielgue, J. Tabbagh, R. Punongbayan, Geophys. Res. Lett. **30**, 1481 (2003)
21. F. H. Weinlich, E. Faber, A. Boušková, J. Horálek, M. Teschner, J. Poggenburg, Tectonophysics **421**, 89 (2006)
22. M. Heiligmann, J. Stix, G. Williams-Jones, B. Sherwood, V.G. Garzón, J. Volcanol. Geotherm. Res. **77**, 267 (1997)
23. M. Cigolini, M. Laiolo, G. Ulivieri, D. Coppola, M. Ripepe, J. Volcanol. Geotherm. Res. **264**, 49 (2013)
24. C. López, et al., Geophys. Res. Lett. **39**, L13303 (2012)
25. G.D. Padilla, et al., Geochem. Geophy. Geosyst. **14**, 432 (2013)
26. M. Trique, P. Richon, F. Perrier, J.P. Avouac, J.C. Sabroux, Nature **399**, 137 (1999)
27. F. Perrier, P. Richon, J. Environ. Radioactiv. **101**, 279 (2010)
28. S. Barbosa, U. Zafrir, U. Malik, O. Piatibratova, Geophys. J. Int. **182**, 829 (2010)
29. C.J. Groves-Kirkby, A.R. Denman, R.G.M. Crockett, P.S. Phillips, G.K. Gillmore, Sci. Total Environ. **367**, 191 (2006)
30. P. Richon, L. Moreau, J.C. Sabroux, E. Pili, A. Salaün, J. Geophys. Res. **117**, B12404 (2012)
31. G. Steinitz, O. Piatibratova, P. Kotlarsky, J. Environ. Radioactiv. **102**, 749 (2011)
32. P.A. Sturrock, G. Steinitz, E. Fischbach, D. Javorsek, J.H. Jenkins. Astropart. Phys. **36**, 18 (2012)
33. G. Steinitz, O. Piatibratova, N. Charit-Yaari, Proc. R. Soc. A. **469**, 20130411 (2013)
34. Consejo Insular de Aguas, Cabildo de Tenerife. Estación de adquisición de datos del sondeo de Las Cañadas del Teide. Internal report, 1998 (unpublished)
35. I. Farrujia, J. Braojos, J. Fernandez, in *Proceedings of the VII Simposio de Hidrogeología de la Asociación Española de Hidrogeólogos* (Murcia, 2001), p. 661

36. A. Woodcock, Bull. Am. Meteorol. Soc. **68**, 125 (1987)
37. G. Li, G., H. Zong, Sci. China Earth Sci. **50**, 1380 (2007)
38. G. Li, H. Zong, Q. Zhang, Adv. Atmos. Sc. **28**, 45 (2011)
39. G. Steinitz, O. Piatibratova, P. Kotlarsky, J. Environ. Radioactiv. **134**, 128 (2014)